# Comparison and optimization of off-axis Phase-Detection Auto-Focus (PDAF) pixels

Q. Haemmerlé*, F. Omeis*, D. Maitre*, J. Chossat*, E. Huss*, O. Jeannin*, D. Rideau*,
A. Crocherie†, H.S. Leong‡, I. Nicholson†, J. Downing†, C. Augier*, J. Favreau*, G. Mugny*
* STMicroelectronics, Technology and Design Platforms and Imaging Division, France
† STMicroelectronics, Imaging Division, United-Kingdom, ‡ STMicroelectronics, Imaging Division, Singapore

***Abstract*—While Phase Detection Auto-Focus (PDAF) pixels are nowadays present in most high-end smartphone cameras, a broad variety of pixel designs are found in recent products, and optimization studies are usually limited to one specific architecture. In this paper, we compare different PDAF designs, such as shielded pixels, 2x1 On-Chip Lens (OCL) and Quad-Bayer architectures, by mean of electromagnetic simulation. We study in detail the PDAF performance of the different designs for different pixel pitches. We use Bayesian optimization to define the best optical stack for each cases, defining a simple Figure-of-Merit, allowing to study the influence of the module objective lens aperture on PDAF performance. Finally, we study the influence of the microlens shift decision on the off-axis performance. This study shows that the best PDAF design depends on many factors, and will help pixel designers to choose the best PDAF designs as a function of their image sensor product.**

## I. Introduction

For many applications, cameras are required to reach focus quickly and accurately, e.g. for filming scenes where objects are moving fast and appear in the foreground. Recent high-end CMOS image sensors usually relies on phase-detection auto-focus (PDAF) pixels, scattered on the image sensor array, which allows the camera to reach the focus two to three times quicker than only relying on standard contrast detection algorithm [1].

The most common PDAF pixel design comprises: (i) pixels shielded by metal lines or back-side metal shields [2] (referred as "shielded PDAF" hereafter); (ii) dual-photodiode under a single microlens [3], [4]; (iii) 2x1 On-Chip Lens (OCL) where specific microlenses are covering two adjacent pixels [5]; (iv) 2x2 OCL, e.g. in Quad-Bayer array [6], [7]; or sometimes a combination of different technics [8] or, recently, plasmonic nanostructures [9] and color router [10].

While (i) and (ii) solutions are suitable for large pitch pixels, (iii) and (iv) options are becoming more popular as the pixel pitch reduces [11]. However, a detailed analysis and comparison of PDAF metrics for different designs and pitches is not straightforward and only a few simulation studies can be found in the literature [12], [13], [14]. Moreover, for an accurate calculation of the phase-shift, on-axis and off-axis PDAF pixels need to have both identical Quantum Efficiency (QE) on focus, and the same disparity sensitivity when out-of-focus.

In this paper, we compare different PDAF pixels designs and propose a simple methodology to evaluate them, including the module optics in a pragmatic way. We discuss off-axis performance in details and show the trade-off for the optimal microlens shift in term of best QE and PDAF performance.

## II. Methodology

To determine the distance and direction to focus, the PDAF algorithm relies on the phase shift between, typically two images. These images comes from angle-sensitive pixels, which are collecting light coming from different part of the entrance pupil. Without lack on generality, we will study here one direction only, referred below as "left" and "right" direction. [1]

To evaluate the performance of PDAF pixels, angular measurement or simulation are usually performed to extract the separation ratio (SR) between left and right PDAF pixels (see Fig. 1) [6]:

$$SR(\theta)_{\theta>0} = \frac{QE_R(\theta)}{QE_L(\theta)}$$

where $QE_L(\theta)$ and $QE_R(\theta)$ are the QE of, resp., the left and right pixels and $\theta$ is the angle of incidence of light, which is defined positive when light propagates towards the left pixel. The angle at which the separation ratio goes below 0.2 defines the accuracy of the PDAF for fine contrast detections.

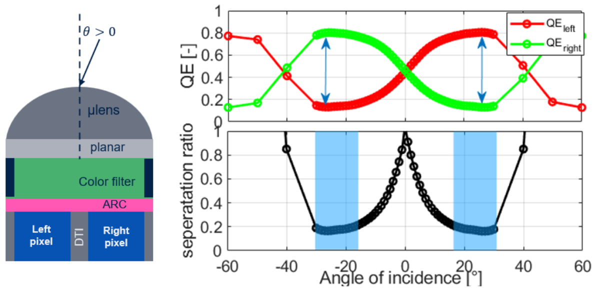


Fig. 1. Angular response (top) and separation ratio (bottom) of left and right PDAF pixels. The blue rectangles show the region where the separation ratio is below 0.2. The schema on the left shows the angle of incidence as a function of left/right pixel position.

[1]N.B.: there could be some naming confusion: e.g. in the case of a 2x1 PDAF pixels, the pixel below the right part of the microlens will actually be sensitive to light coming from the left part of the entrance pupil, when focus occurs in front of the sensor. Here, we choose to name the pixel according to the physical position of its sensitive area: in the example above, the pixel would be referred as "right" PDAF pixel and its angular response as $QE_R(\theta)$.

979-8-3195-0631-3/26/$31.00 ©2026 IEEE

A novel approach was recently proposed, to extract the disparity sensitivity by fully coupled ray tracing and electromagnetic simulation framework [12]. This disparity sensitivity includes contributions from many sources, such as the main objective lens aperture, the image signal processing algorithm, as well as the pixel pitch and design.

While the methodology in [12] is accurate, it requires a predefined objective lens design and is not suited for running fast and efficient optimization on a broad range of parameters. Here, we define a general Figure-of-Merit (FoM) inspired by the separation ratio metric, but extended to off-axis:

$$FoM = \frac{1}{N_\theta}\left(\sum_{\theta=CRA-\theta_f}^{CRA}\frac{T_L(\theta)}{T_R(\theta)} + \sum_{\theta=CRA}^{CRA+\theta_f}\frac{T_R(\theta)}{T_L(\theta)}\right) \quad (1)$$

where $CRA$ is the Chief-Ray Angle considered, $\theta_f$ is the boundary of the illumination cone defined by the module lens, $N_\theta$ is the number of simulations within the illumination cone $[CRA-\theta_f : CRA+\theta_f]$, and $T_R$ and $T_L$ are the transmission on the right and left PDAF pixel, respectively.

In this study, the light propagation and absorption in PDAF pixels is studied by 3D electromagnetic simulations, solving Maxwell equation with either Finite-Difference Time Domain (FDTD) method, or Rigourous Coupled-Wave Analysis (RCWA). FDTD simulations are performed with Lumerical software, commercialized by Synopsys-Ansys [15], while RCWA simulations are done with our *in-house* tool.

For all simulations, we consider a plane wave illumination at 530nm wavelength with different angles of incidence. Green pixel is chosen as a reference, but the same methodology can be applied to any wavelength. The optical stack parameters and microlens radial shift are first optimized by RCWA methods, coupled with Bayesian optimization as implemented in Turbo package [16], [17], considering an illumination cone of $\pm 14°$ (corresponding to F/2). For efficient simulation time, we stop the simulation on the top of Si substrate and we consider that each photon transmitted will be absorbed and converted into a useful signal. This approximation is valid in visible light, as all the signal is absorbed within the first part of the substrate and metal lines don't play a role in the optical propagation. However, the presence of Deep Trench Isolation (DTI) within the Si substrate can modify the results slightly. For this reason, the refined QE angular response is then computed by FDTD on the full-pixel, including DTI and 6$\mu$m Si epitaxy thickness.

Different PDAF pixels designs are studied, as shown in Fig. 2. We consider a standard Back-Side Illuminated pixel with a microlens, colour filter array and anti-reflective coating on top of Si substrate. Fig. 3 gives all the optical stack details with layer thickness's and materials. The microlens is defined by three parameters: its height, pitch and lens intersection (see Fig. 3), which are optimized for best performances, together with the planar thickness.

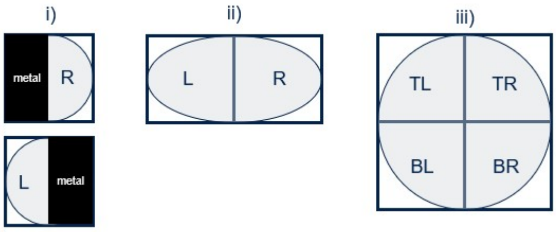


Fig. 2. Schematic top view of three different PDAF pixel designs: (i) shielded pixel (ii) 2x1 OCL and (iii) 2x2 OCL (light grey circular shapes are illustrating the microlens area).

| Stack name | Thickness [nm] | Materials name** |
|---|---|---|
| TopCoat | 100 | SiO |
| Microlens | TBD* | Microlens resist |
| Planar | TBD* | Microlens resist |
| CFA | 600 | Color resist |
| ARC 3 | Thickness 3 | Oxide 3 |
| ARC 2 | Thickness 2 | Oxide 2 |
| ARC 1 | Thickness 1 | Oxide 1 |
| Substrate | 6,000 | Si |

*see Table 4 for optimized values.
**all (n,k) values come from our internal database.

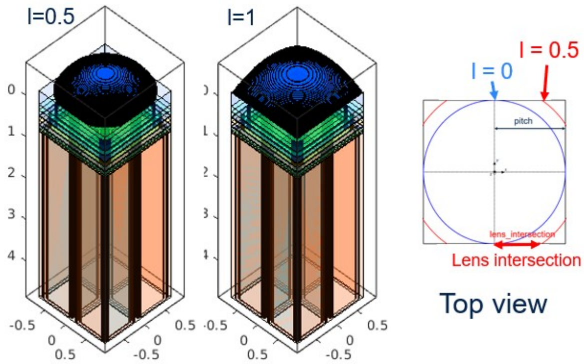


Fig. 3. (Top) table of the optical stack parameters. In the case of shielded pixel, a 200nm-thick W layer is added within the CFA layer. This layer also serves as a isolation wall between color filters, in the case of 2x2 OCL Quad-Bayer. (Bottom) two examples of optical stack of the 2x2 OCL pixels with a microlens height of 200nm and a lens intersection of 0.5 (left) and 1 (middle). A top view schematic illustrating the definition of lens intersection is also shown on the right.

## III. Results and Discussion

### A. PDAF design comparison

Firstly, the optical stack for a 1$\mu$m pixel pitch was optimized, with RCWA and Bayesian optimization, for (i) shielded, (ii) 2x1 OCL and (iii) 2x2 OCL PDAF designs. The optimal optical stack parameters are given in Table 4.

| Stack Parameter | Design (i) | Design (ii) | Design (iii) |
|---|---|---|---|
| Microlens height [nm] | 550 | 550 | 1,130 |
| Microlens intersection [-] | 0.1 | 0.1 | 0.9 |
| Planar [nm] | 300 | 300 | 380 |

Fig. 4. Optimal optical stack parameters found by Bayesian optimisation, for on-axis performance at 530nm and F/2 for the three designs defined in Fig. 2.

The angular response of on-axis PDAF pixels is shown in Figs. 5. The performances of the colour router design from [10] is also presented for comparison.

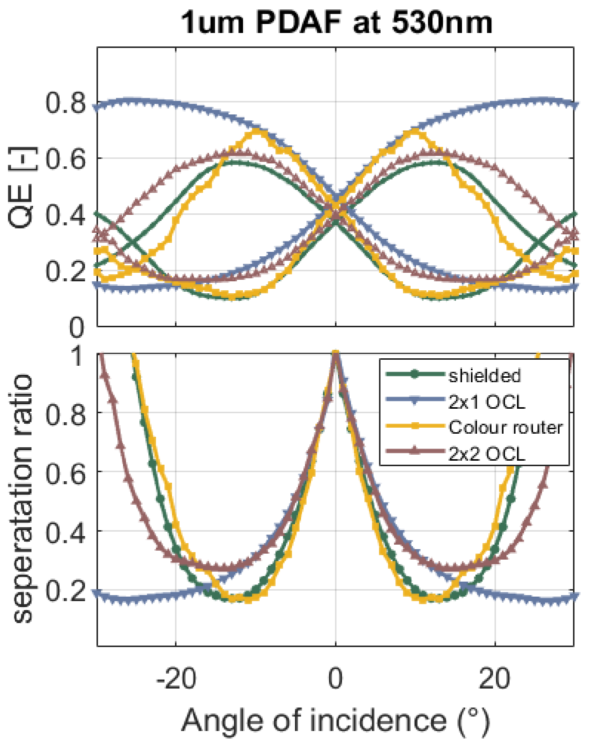


Fig. 5. QE angular response and separation ratio of on-axis 1$\mu$m PDAF pixels, comparing four different architectures: shielded, 2x1 OCL, 2x2 OCL and colour router from Ref. [10], with optimized optical stack.

When comparing the different designs, for this small pixel pitch, we can see that, even after careful optimization, they are still performing differently, and they all have pros and cons.

The overall QE is smaller for the shielded PDAF, as expected, due to the absorption by metal shield. However, the separation ratio drops faster and reaches values below 0.2 between 10 and 15°, while 2x1 PDAF has a separation ratio below 0.2 only for angles higher than 20°.

Note that, in the case of shielded PDAF, transmission on top of Si and volume absorption are almost identical. However, in the cases of 2x1 and 2x2 OCL, the presence of DTI in the center of the microlens can affect the results, which reduces the crosstalk between the left and right pixels, but also the sensitivity at normal incidence. This can be seen in Fig. 6, which plots a cross-section of the Poynting vector at 10° incidence angle, for the shielded and 2x1 OCL pixels. For the 2x1 OCL, light hits the DTI that separates the two pixels and is scattered, while higher separation ratio is obtained by shielded PDAF.

The loss of QE due to the DTI is also illustrated in Fig. 7, in the case of a 2x2 OCL. It compares the light transmission at the Si top and the volume absorption, as a function of the $\theta$ and $\phi$ incidence angles, adding the signal of the four Quad-

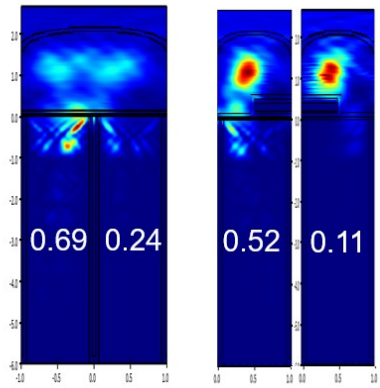


Fig. 6. 2D cross-section of the Poynting vector for an angle of incidence of 10° in 2x1 OCL (left) and shielded (right) pixels. Values in white give the QE of each pixels.

Bayer pixels. To overcome the QE loss due to DTI at the center of the microlens, some solutions are proposed in the literature, e.g. by creating a DTI opening at the center of the pixel [12]. As discussed in previous studies [10], the color router are also promising solutions, not only for increased QE, but also for better PDAF performances in their Quad-Bayer implementations.

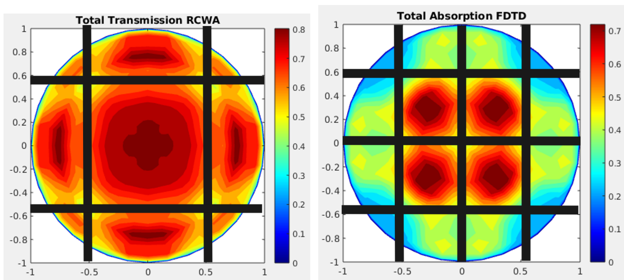


Fig. 7. 2D maps of summed signal of the four 2x2 OCL Quad-Bayer pixels: (left) RCWA transmission at Si top and (right) FDTD volume absorption. Black lines are highlighting the effect of isolation walls and DTI. The crosstalk and the sensitivity at normal incidence (at the center of the plot) are both strongly reduced in the right figure, due to the presence of DTI.

It ought to be mentioned that the Figure-of-Merit, as defined in Eq. 1, also depends on the module lens aperture and the optical stack is optimized here for F/2 only. Using the same pixel with different module lens may give better, or poorer, Figure-of-Merit, as shown in Fig. 1. Specifically, as the separation ratio for the 2x1 OCL remains low for angles beyond 20° (see Fig. 5), it outperforms the other architectures for F/# below 1 in Fig. 8.

## *B. Off-axis performances*

For off-axis pixels, the optimal microlens shift is originally defined so that the QE shows a flat response at any position in the array. PDAF pixel bring an additional constraint: left and right pixels must have the same signal at any position, when

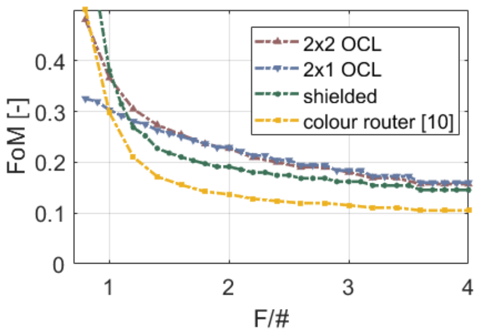


Fig. 8. Figure-of-Merit versus F/# for on-axis performance of Fig. 5. The lower the Figure-of-Merit, the best performing the pixel.

on-focus, and their Figure-of-Merit shall not deteriorate from on-axis.

For 1$\mu$m pixel pitch, optimal radial shift rate is 18 nm/° for a flat QE at 530nm (see Fig. 9). For the same pixel, the optimal radial shift rate oscillates between 18, 24 and 34 nm/° for, resp., the shielded, 2x1 and 2x2 OCL PDAF pixels, for matching left and right QE (see Fig. 10). Finally, the effect of different radial shift rate on the PDAF Figure-of-Merit is shown in Fig. 10. While the non-optimal rate of 18 nm/° shows a deterioration of its off-axis Figure-of-Merit compared to 24 nm/°, the 2x1 OCL still outperforms the shielded PDAF architecture, which deteriorate strongly off-axis.

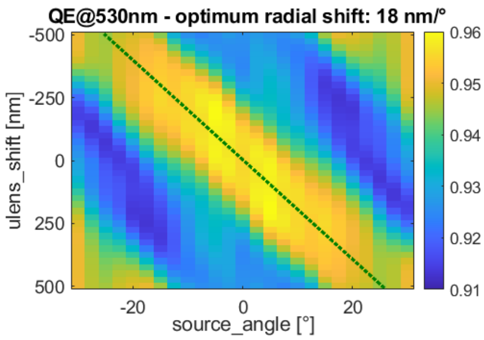


Fig. 9. QE at 530nm versus source angle and microlens shift. The green dashed line shows the optimal radial shift rate of 18 nm/°.

## IV. Conclusion

This paper compares the PDAF performances of three different designs for a 1$\mu$m pitch pixel: shielded, 2x1 and 2x2 OCL. While the optical stack is optimized in each case, the PDAF performances at F/2 show discrepancies and the shielded PDAF shows best separation ratio and Figure-of-Merit. However, this architecture shows a strong Figure-of-Merit deterioration off-axis, and a loss of QE due to absorption of metal shield. We believe that this comparison can help pixel designers choose an appropriate and best-performing PDAF pixel architecture, adapted to their use-case. The same

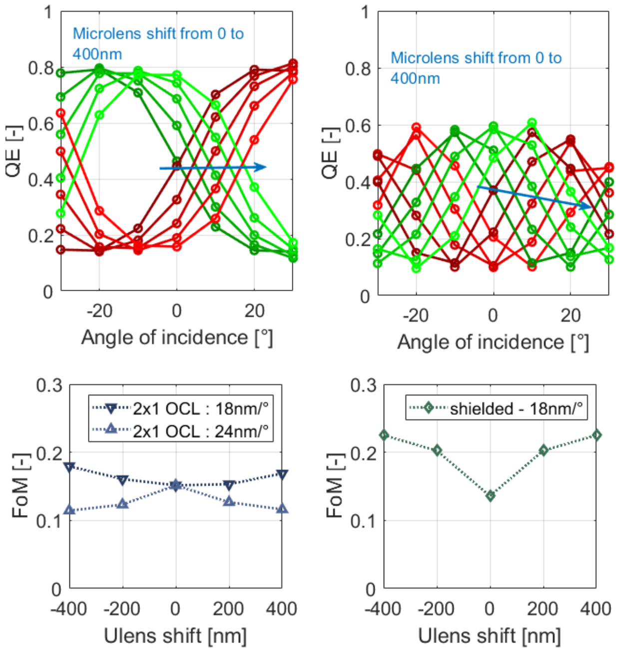


Fig. 10. (Top) QE variation of the left (in red) and right (in green) pixel for different microlens shifts, sweeping from 0 to 400nm with a step of 100nm, as function of source angle of incidence for: (top left) 2x1 OCL and (top right) shielded PDAF. The points where left and right QE crosses are defining an optimal radial shift rates of 24 and 18 nm/°, for 2x1 and shielded respectively. (Bottom) Figure-of-Merit for different radial shift rates.

methodology can also be applied to more exotic designs and a detailed study of the impact of the pixel pitches will be presented at the conference.

## References


[1] P. Robisson *et al.*, *Electronic Imaging*, vol. 29, pp. 209–218, 2017.

[2] B.-S. Choi *et al.*, in *2018 IEEE International Conference on Imaging Systems and Techniques (IST)*. IEEE, 2018, pp. 1–5.

[3] S. Yokogawa *et al.*, in *2015 Int. Image Sensor Workshop*, 2015, pp. 1–04.

[4] D. Shirahige *et al.*, in *2023 International Electron Devices Meeting (IEDM)*. IEEE, 2023, pp. 1–4.

[5] D. Keum *et al.*, in *2021 International Conference on Solid State Devices and Materials*, 2021.

[6] T. Okawa *et al.*, in *2019 IEEE International Electron Devices Meeting (IEDM)*. IEEE, 2019, pp. 16–3.

[7] J. Lee *et al.*, in *Proceedings of the Int'l Image Sensor Workshop (IISW)*, 2023, pp. 68–71.

[8] K. Kikuchi *et al.*, in *2024 IEEE SENSORS*. IEEE, 2024, pp. 1–4.

[9] G. Seok *et al.*, *IEEE Sensors Journal*, 2025.

[10] J. Go *et al.*, in *2025 IEEE International Electron Devices Meeting (IEDM)*. IEEE, 2025, pp. 1–4.

[11] J. Scott-Thomas, in *2023 International Image Sensor Workshop*, 2023.

[12] E. Song *et al.*, in *2025 International Conference on Simulation of Semiconductor Processes and Devices (SISPAD)*. IEEE, 2025, pp. 1–4.

[13] M. Kobayashi *et al.*, *Japanese Journal of Applied Physics*, vol. 57, no. 10, p. 1002B5, 2018.

[14] G. Chataignier *et al.*, *Optics Express*, vol. 27, no. 21, pp. 30 486–30 501, 2019.

[15] Lumerical, *Inc., 2024-r2 edition*, 2024.

[16] D. Eriksson *et al.*, *Advances in neural information processing systems*, vol. 32, 2019.

[17] D. Maitre *et al.*, in *2025 International Conference on Simulation of Semiconductor Processes and Devices (SISPAD)*. IEEE, 2025, pp. 1–4.